Investigating The Starburst-AGN Connection

Thomas Nikola

Gordon Stacey, Henrik Spoon
(Cornell University)

Outline

- Luminous Infrared Galaxies (LIRGs, ULIRGs, HyLIRGs)
- Power Source
- Galactic Nuclei
- Starburst/AGN diagnostics
- Merger Sequence
- Secular Evolution
- Starburst-AGN Evolution
- Mid-J CO Probes
- Mid-IR Probes; SED Decomposition
- FORCAST/SOFIA
- Observation of NGC 3227
- Future SOFIA Observations/Instrumentation

Infrared Luminous Galaxies

- LIRGs: 10^{11} L_{sun} < L_{IR} < 10^{12} L_{sun}
- ULIRGs: 10^{12} L_{sun} < L_{IR} < 10^{13} L_{sun}
- HyLIRGs: 10^{13} L_{sun} < L_{IR}
- Classification is purely due to L_{IR}
- Classification does not necessarily specify a certain galaxy type or class
- Only requirements:
  - Dusty
  - Powerful heating mechanism

Local "ULIRGs": Strongly Interacting/Merging Galaxies

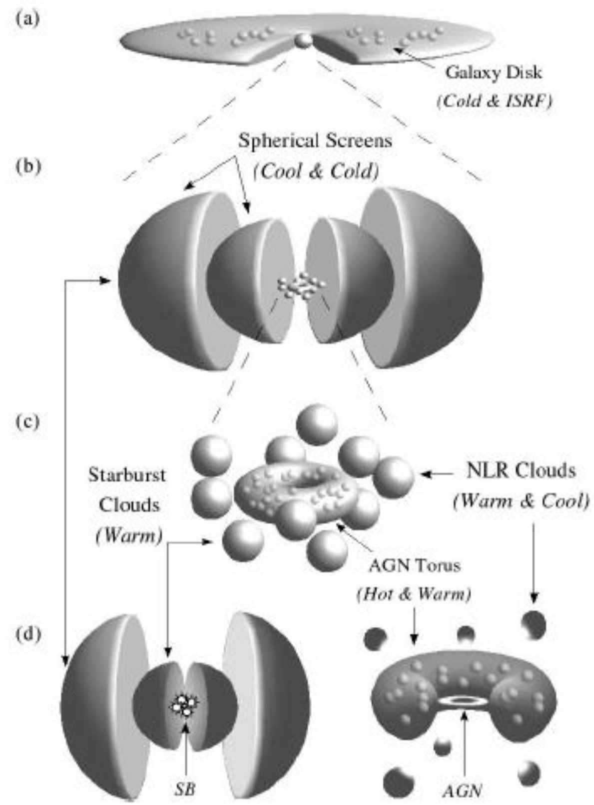

Marshall et al. 2007, ApJ, 670, 129

High-z “ULIRGs”

- Interacting/Merging Galaxies with AGN and/or enhanced star formation rate (high efficiency)
- Gas rich galaxies with “normal”/standard star formation efficiency

ULIRG Power Source: Starburst/AGN Diagnostics

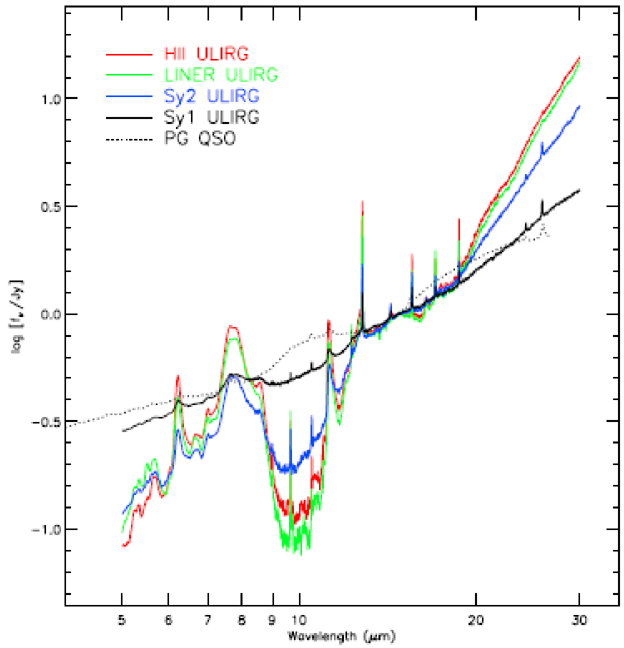

Figure 9. Average IRS spectra for ULIRGs of various optical spectral types, compared with the QSOs in our sample. The individual spectra in each category were normalized to have the same rest-frame 15 μm flux density. Note the similarity between the average spectrum of Seyfert 1 ULIRGs and that of QSOs.

Veilleux et al. 2009, ApJS, 182, 628

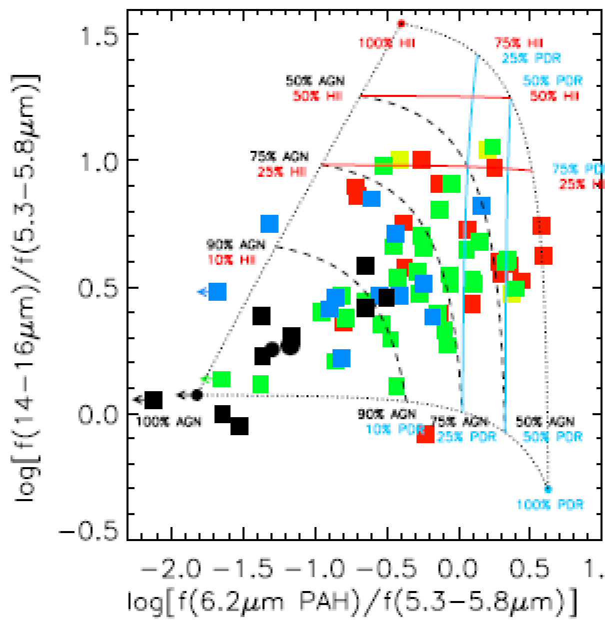

Figure 34. AGN/H II/PDR mixing diagram based on the Laurent et al. (2000) method, as modified by Armus et al. (2007): PAH (6.2 μm) to continuum (5.3–5.8 μm) flux ratios vs. the continuum (14–16 μm)/(5.3–5.8 μm) flux ratios. The meaning of the symbols is the same as in Figure 4. The zero points for the pure H II region (upper-right) and PDR (lower-right) are from Armus et al. (2007) and the zero point for the pure AGN (lower-left) corresponds to the average value for the FIR-undetected PG QSOs to reduce possible starburst contributions to the continuum emission (Paper II). *Note that the percentages included here are percentages of the* 5.3–5.8 μm *continuum*; actual AGN fractional contributions to the bolometric luminosities will be lower.

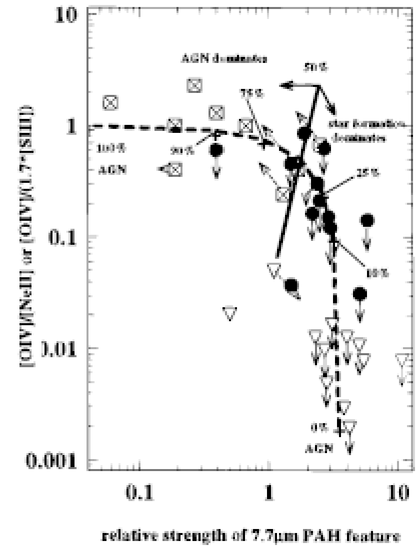

Genzel et al. 1998, ApJ, 498, 579

ULIRG Power Source: Starburst/AGN Diagnostics

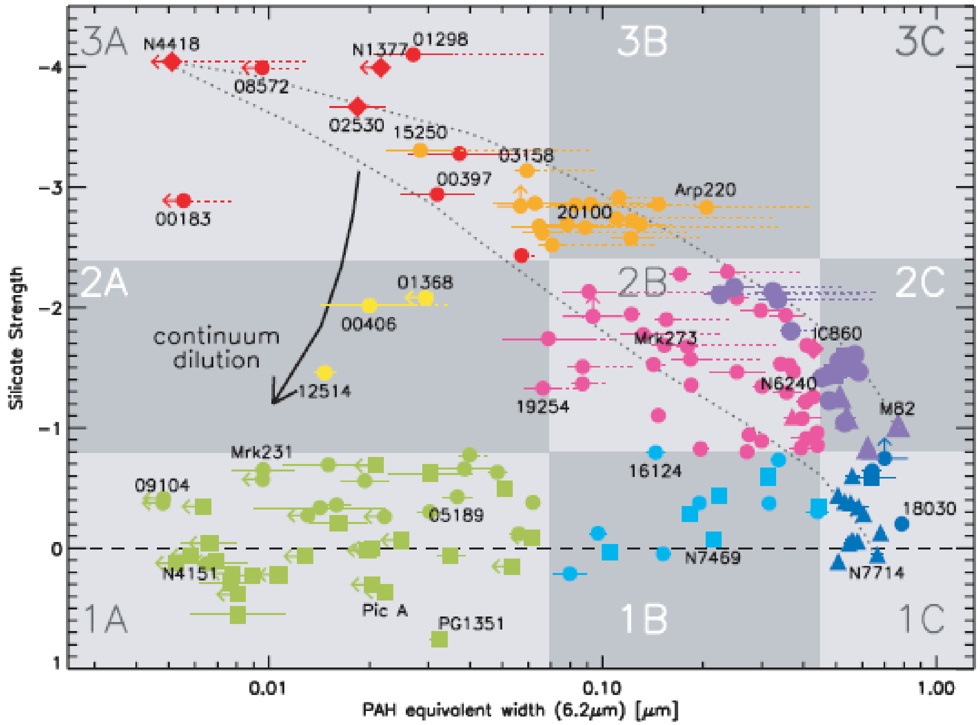

Fig. 1.—Diagnostic plot of the equivalent width of the 6.2 micron PAH emission feature vs. the 9.7 mm silicate strength. Upper and lower limits are denoted by arrows. The galaxy spectra are classified into nine classes (identified by nine shaded rectangles) based on their position in this plot. Colors are used to distinguish the various classes. From class 1A to 1B, 1C, 2A, 2B, 2C, 3A, and 3B the colors used are green, cyan, dark blue, yellow, pink, purple, red, and orange. After class assignment the PAH equivalent widths were corrected for the effect of 6 micron water ice absorption on the 6.2 micron continuum. The extent of the individual corrections are indicated by dotted horizontal lines. The two dotted black lines are mixing lines between the spectrum of the deeply obscured nucleus of NGC 4418 and the starburst nuclei of M82 and NGC 7714, respectively. Galaxy types are distinguished by their plotting symbol: Filled circles: ULIRGs and HyLIRGs. Filled triangles: Starburst galaxies. Filled squares: Seyfert galaxies and QSOs. Filled diamonds: Other infrared galaxies.

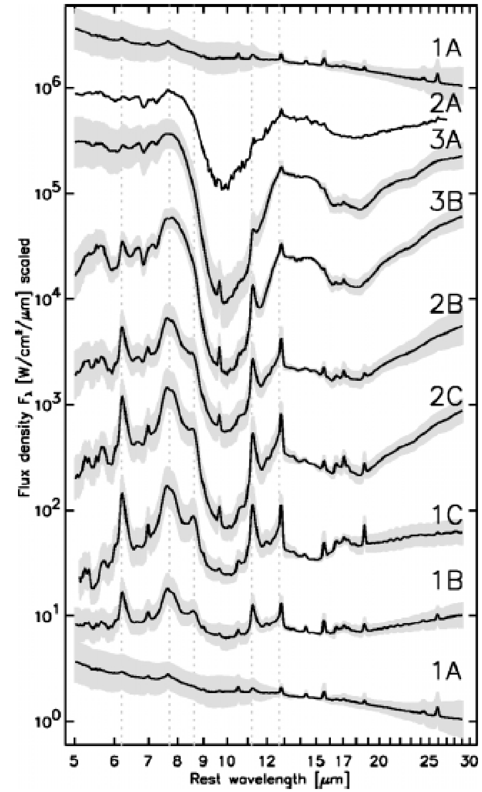

Spoon et al. 2007, ApJL, 654, L49

ULIRG "Classes"

- "Classes" mainly determined by extinction/obscuration effects and PAH equivalent widths
- ULIRG AGN classes:
  - Veilleux et al. 2009, ApJS, 182, 628
  - Class 1:
    - PAH EqW: starburst-dominated;
    - extinction: small;
  - Class 2:
    - PAH EqW: starburst-dominated, but strong AGN contribution
    - extinction: large;
  - Class 3:
    - PAH EqW: small; AGN contribution ≥ starburst contribution;
    - extinction: small;

Merger Sequence

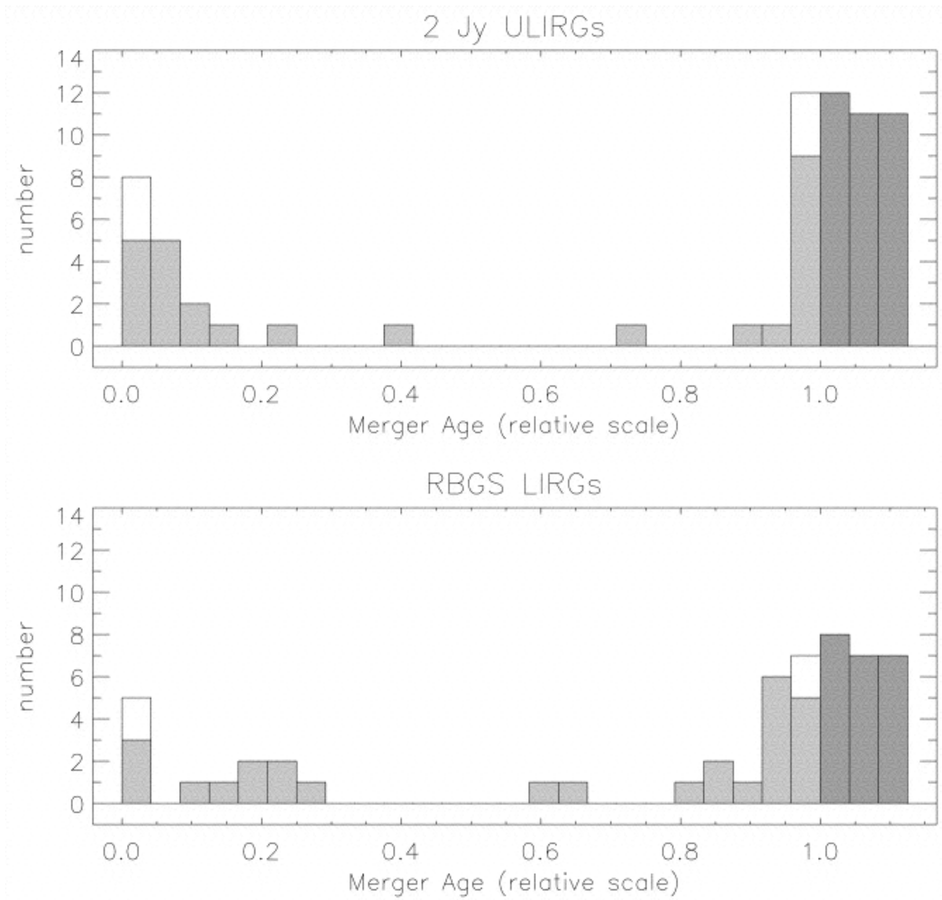

- At age = 0: initial encounter
- At age = 1: final merger
- Unit 1 ~ 10^9 yr

Murphy et al. 2001, ApJ, 559, 201

Merger Sequence

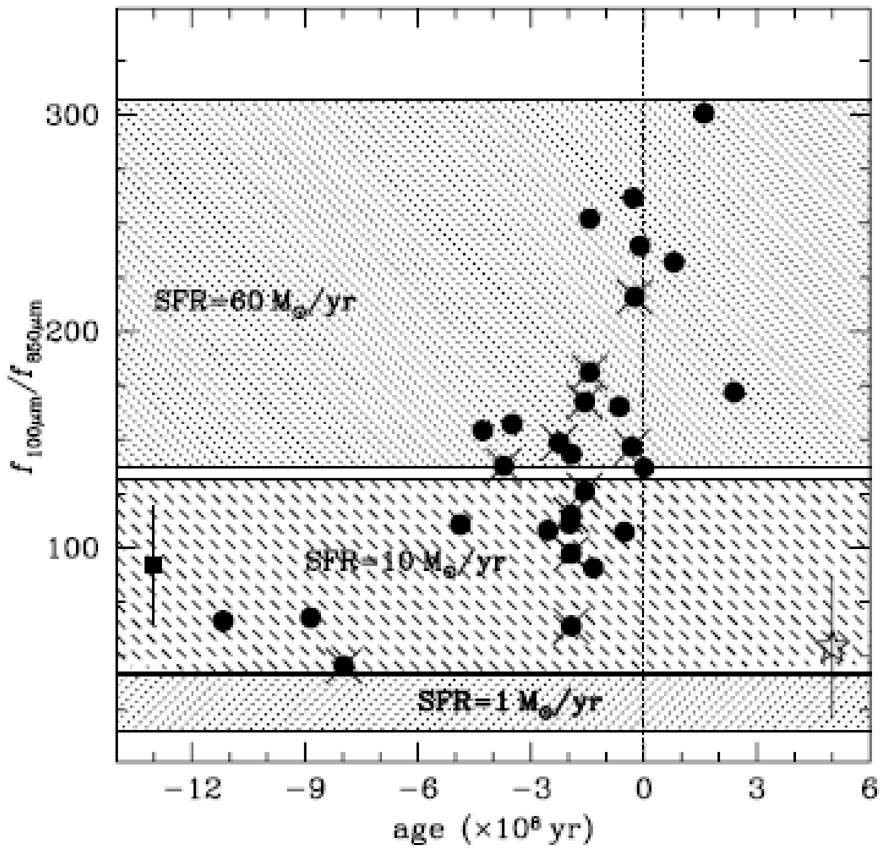

Figure 3. The f_{100}/f_{850} flux ratio plotted against the age parameter for our sample of interacting galaxies. The full circles are the interacting galaxy sample in this study. A cross on top of a symbol signifies an AGN in the catalogue of Veron-Cetty & Veron (2003). The square corresponds to the mean f_{100}/f_{850} of isolated spirals from the sample of Misiriotis et al. (2004) arbitrarily plotted at an age parameter of −13. The star is the mean f_{100}/f_{850} of ellipticals from the sample of Temi et al. (2004; see text for details) arbitrarily plotted at an age parameter of +5.

Xilouris et al. 2004, MNRAS, 355, 57

Merger Sequence

- Linking start of enhanced star formation activity to specific state in interacting/merging galaxies is not straight forward since it depends on:
  - Encounter geometry
  - Bulge vs. bulgeless system
  - Gas content/mass (“dry” vs. “wet”)

Evolutionary Sequence

- $M_{BH} \sim \sigma_{bulge}$ relation suggests co-evolution of BH growth and nuclear star formation

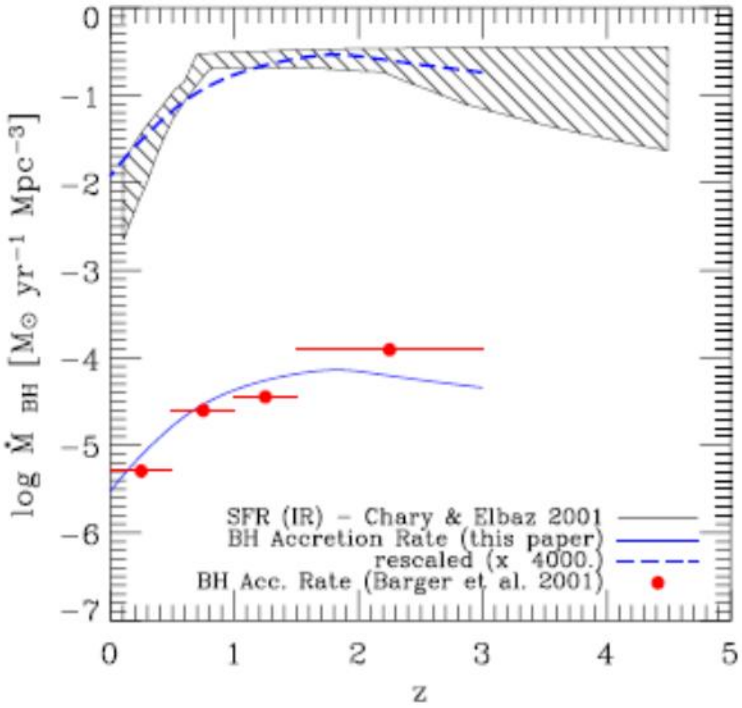

Figure 9. Cosmic BH accretion history compared with the estimate by Barger et al. (2001) and with the cosmic star formation rate by Chary & Elbaz (2001).

Marconi et al. 2004, MNRAS, 351, 169

Evolutionary Sequence

- ULIRG Veilleux classes (1)-(2)-(3) seem to follow a morphological trend suggesting: ULIRG → QSO evolution sequence, but large scatter
- Not clear if a general/default trend exist from ULIRG-starburst → ULIRG-AGN (or vice versa)
- Circum-nuclear starburst could remove angular momentum and gas could subsequently fall toward nucleus and accrete on BH, or
- AGN outflow could quench circum-nuclear starburst, or
- AGN jet could trigger starburst in surrounding gas

AGN Triggers Starburst

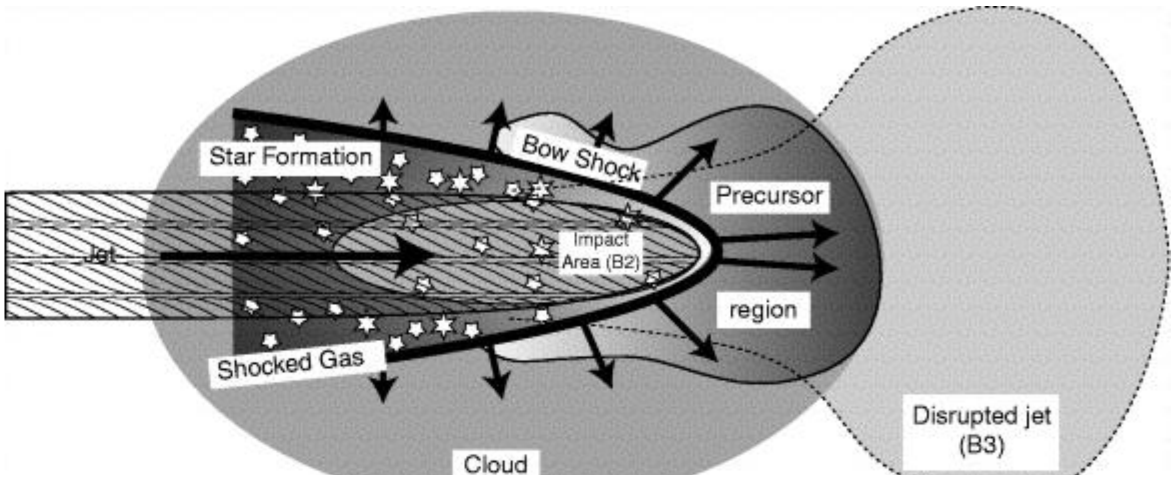

THE ASTROPHYSICAL JOURNAL, 540:678–686, 2000 September 10

JET-INDUCED EMISSION-LINE NEBULOSITY AND STAR FORMATION IN THE HIGH-REDSHIFT RADIO GALAXY 4C 41.17

GEOFFREY V. BICKNELL,[1] RALPH S. SUTHERLAND,[1] WIL J. M. VAN BREUGEL,[2] MICHAEL A. DOPITA,[1]
ARJUN DEY,[3] AND GEORGE K. MILEY[4]
Received 1998 June 8; accepted 2000 April 13

ULIRG Evolution

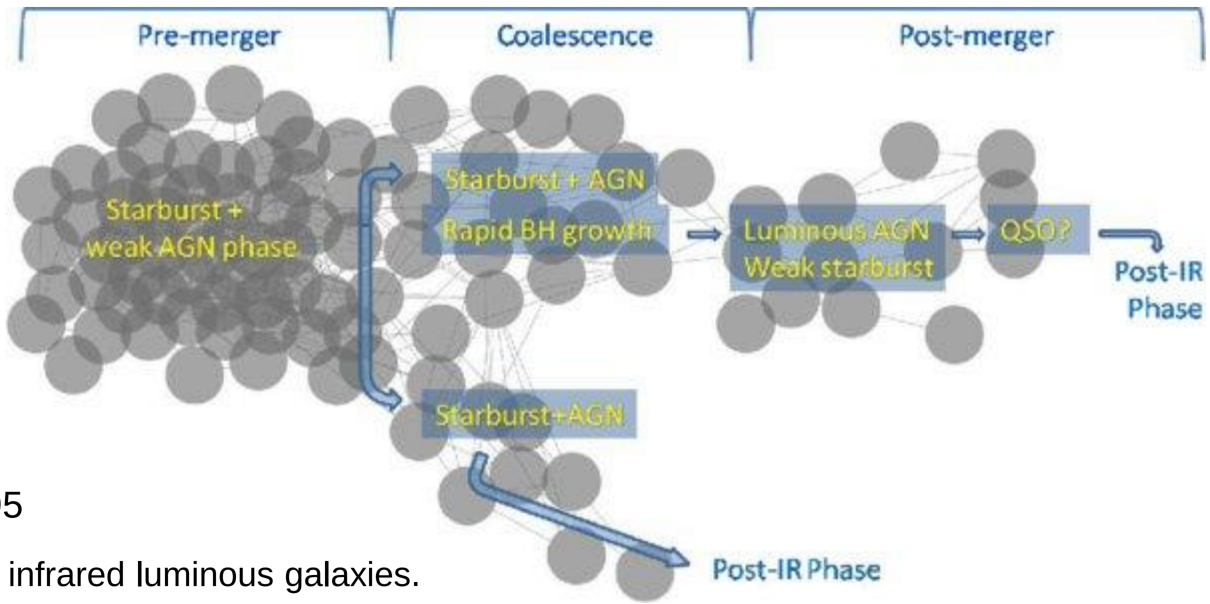

Farrah et al. 2009, ApJ, 700, 395

Evolutionary paradigm for z < 0.4 infrared luminous galaxies.

Three phases in ULIRG lifecycle:

1) from the initial encounter until approximately coalescence:

- homogeneous mid-IR spectral shapes
- mainly from star formation with small AGN contribution possible

Then “ULIRG enters one of two evolutionary paths depending on the dynamics of the merger, the available quantities of gas, and the masses of the black holes in the progenitors”:

2a) contribution from the starburst to the total IR luminosity declines while contribution from the AGN increases; The IR spectral shapes are heterogeneous, likely due to feedback from AGN-driven winds.

3a) “Some objects go through a brief QSO phase at the end.”

2b) “decline of the starburst relative to the AGN is less pronounced”

3b) “few or no objects go through a QSO phase.”

ULIRG Evolution

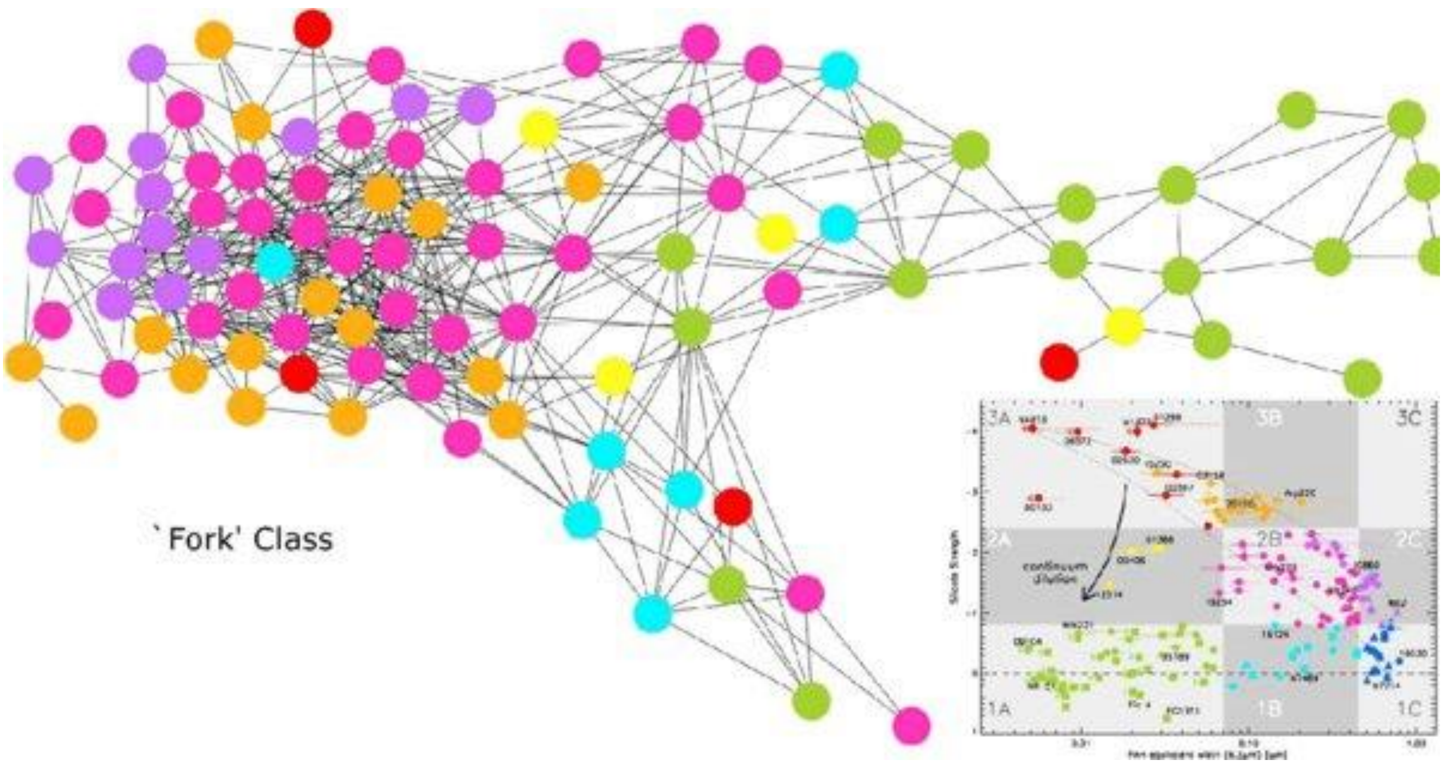

Farrah et al. 2009, ApJ, 700, 395

Starburst-AGN Investigation

- Estimate AGN/starburst contribution as function of galacto-centric distance (zone of influence)
- Excitation mechanisms:
  - Stellar (PDR)
  - AGN (XDR)
  - Outflows/jets (shocks, turbulence, velocity information)

Mid-J CO: PDR

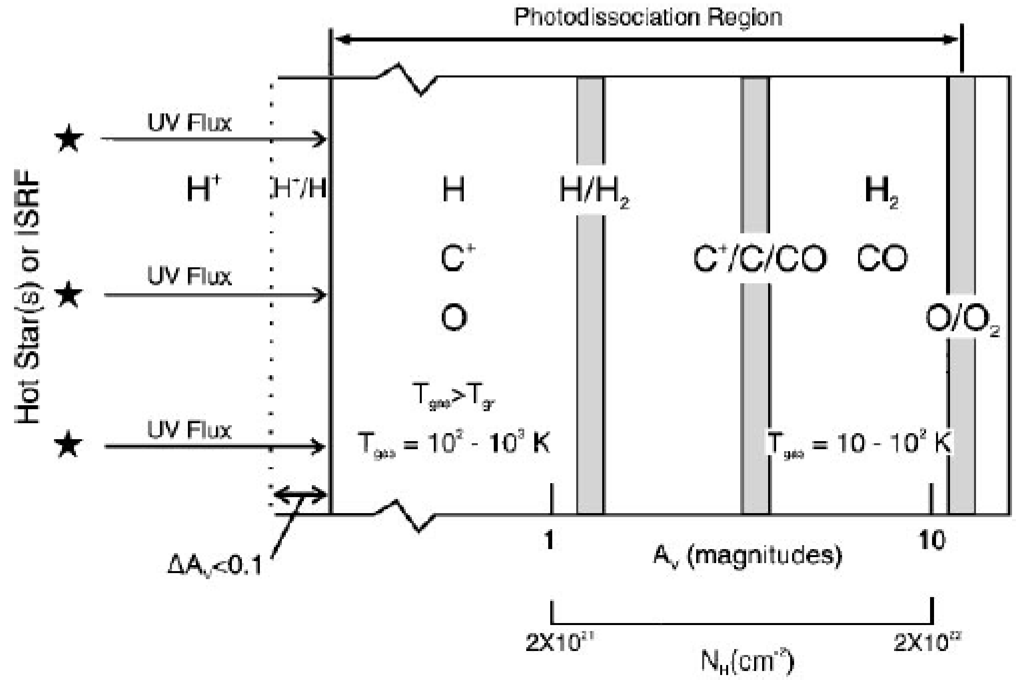

Figure 3 A schematic diagram of a photodissociation region. The PDR is illuminated from the left and extends from the predominantly atomic surface region to the point where O_2 is not appreciably photodissociated ($\simeq$10 visual magnitude). Hence, the PDR includes gas whose hydrogen is mainly H_2 and whose carbon is mostly CO. Large columns of warm O, C, C^+, and CO and vibrationally excited H_2 are produced in the PDR. The gas temperature T_{gas} generally exceeds the dust temperature T_{gr} in the surface layer.

Hollenbach & Tielens 1997, ARA&A, 35, 179

Mid-J CO: XDR

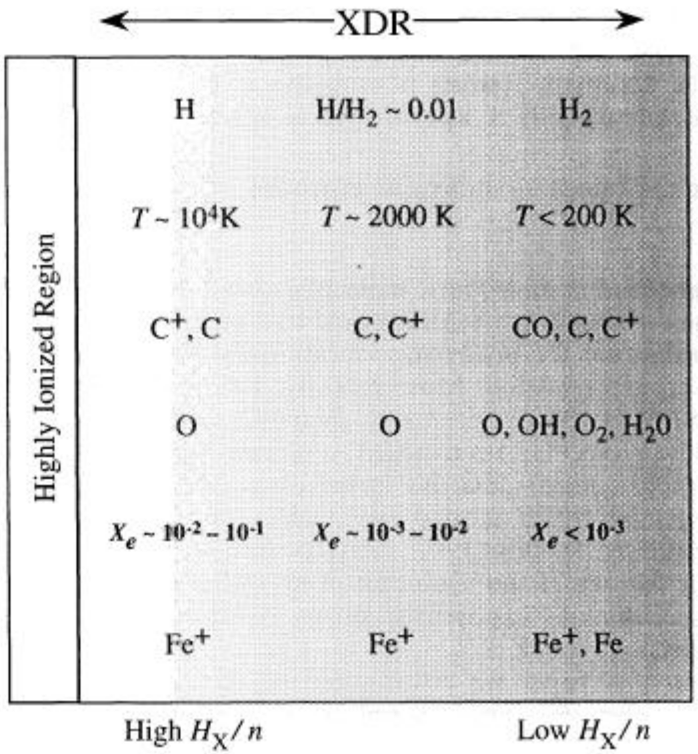

FIG. 1.—Schematic structure of an X-ray dissociation region (XDR). The approximate temperature, chemical composition, and ionization fraction are shown as a function of the ratio of the local X-ray energy deposition rate per particle H_X to the total hydrogen density n (see § 2.1.1). The X-ray flux-to-density ratio decreases from left to right. At very high values of H_X/n (which we do not consider), there will be a highly ionized surface region in which any ionizing UV continuum is also absorbed. If a high column density cloud is exposed to a sufficiently intense X-ray continuum, this schematic XDR will approximate the actual structure of the cloud, with H_x/n decreasing because of absorption with increasing column density into the cloud. Such a gradient in H_X/n will also result from, e.g., increasing distance from an X-ray source, as in the case of molecular clouds in the disk of a galaxy containing an active nucleus.

Maloney, Hollenbach, & Tielens 1996, ApJ, 466, 561

Mid-J CO: Shocks

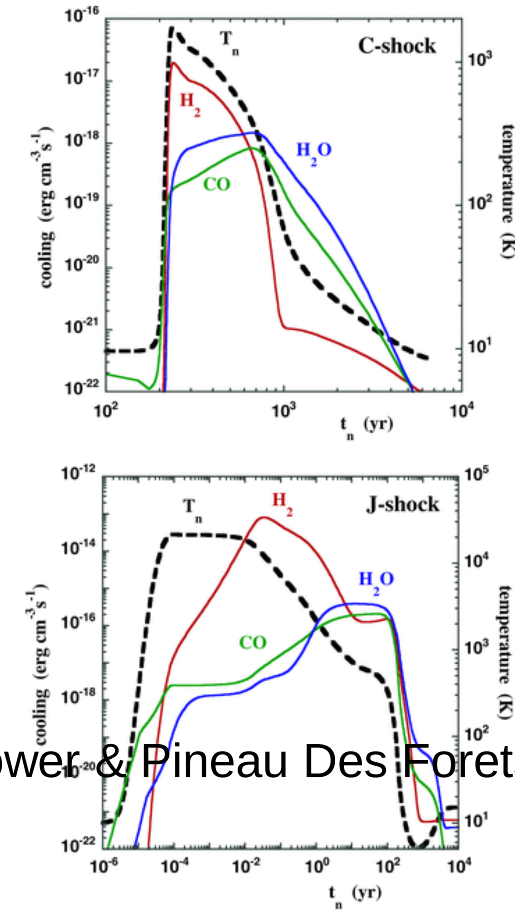

Flower & Pineau Des Forets 2010, MNRAS, 406, 1745

Figure 2. Rates of cooling of the principal molecular coolants through C- and J-type shock waves of speed $v_s = 20\,\mathrm{km\,s^{-1}}$ and initial density $n_H = n(H) + 2n(H_2) = 2 \times 10^4\,\mathrm{cm^{-3}}$. The independent variable is the flow time of the neutral fluid (in connection with the C-type model, which is multifluid).

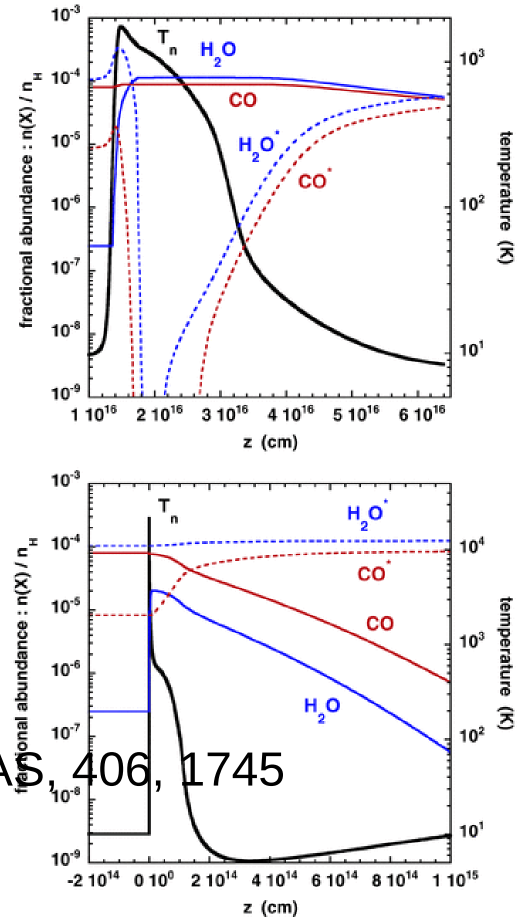

Figure 3. Profiles of selected oxygen-containing species through C-type (upper panel) and J-type (lower panel) shock waves of speed $v_s = 20\,\mathrm{km\,s^{-1}}$ and initial density $n_H = n(H) + 2n(H_2) = 2 \times 10^4\,\mathrm{cm^{-3}}$. An asterisk on a chemical symbol denotes a species in the grain mantles (broken lines). The distance, z, is measured along the direction of propagation of the shock wave.

Mid-J CO: Excitation Diagnostics

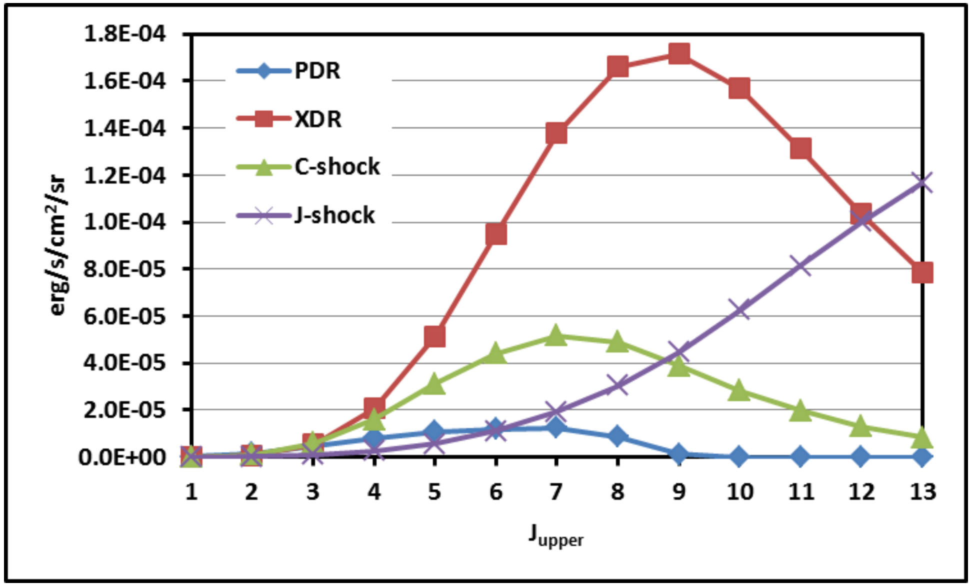

Predicted intensities of rotational CO transitions for PDR and XDR (Meijerink & Spaans 2005, Meijerink, Spaans, & Israel 2006) and shocks (Flower & Pineau Des Forets 2010). The model predictions are for a density of log(n)=4.25, Go=1000, Fx = 16 erg/s/cm2, and v(C-shock)=10km/s, v(J-shock)=20km/s.

Decomposing Dust SED

Example SEDs of emission from the hot, warm, cool, and cold dust components for typical characteristic temperatures of T = 1400, 200, 80, and 35 K (black lines). Also shown are the SEDs obscured by screens (gray lines) having $\tau_{9.7}$ = 1, 2, and 3 (top to bottom).

(Marshall, J.A., et al. 2007, ApJ, 670, 129)

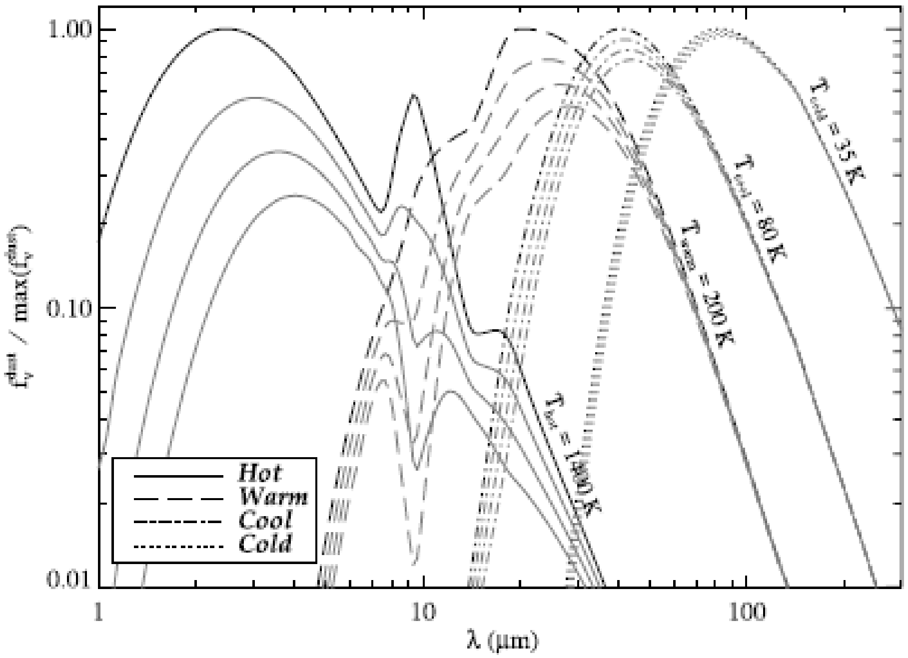

Decomposition of PAH Features

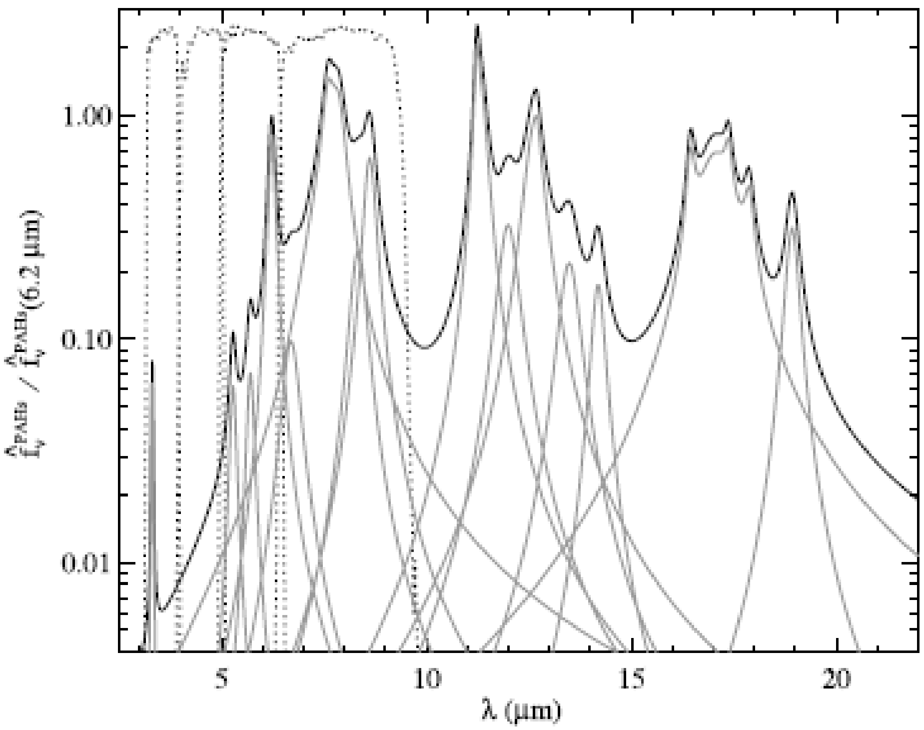

Fig. 8.—PAH emission template (black line) derived from the spectrum of the mean starburst galaxy from Brandl et al. (2006). The individual complexes (gray lines) are modeled with Drude profiles (see Smith et al. 2007). Note the significant “continuum” emission created by the addition of flux in the wings of the broad features. Also shown for reference are the four arbitrarily scaled IRAC transmission curves.

Marshall, et al. 2007, ApJ, 670, 129

SED Decomposition

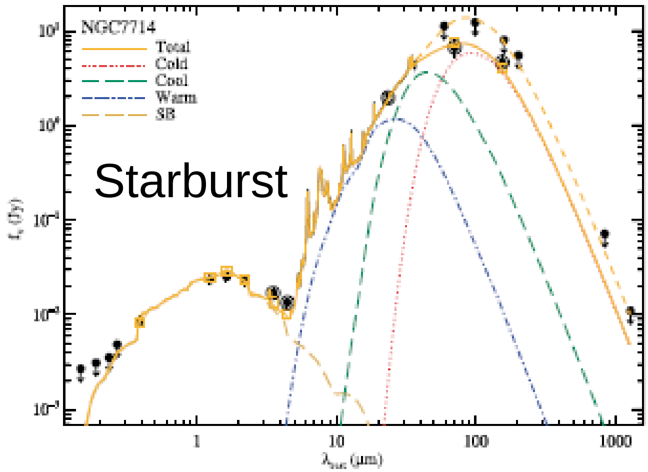

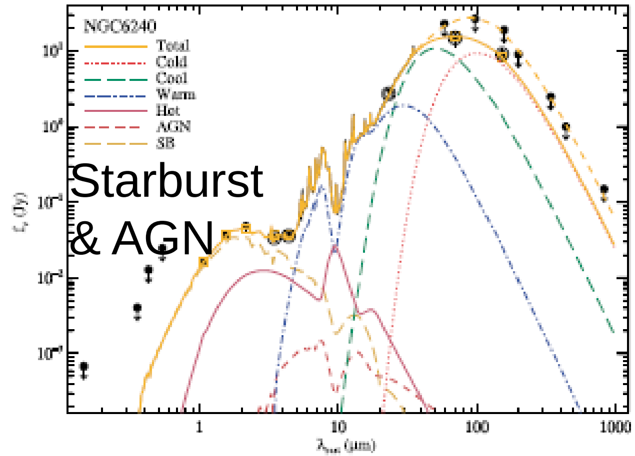

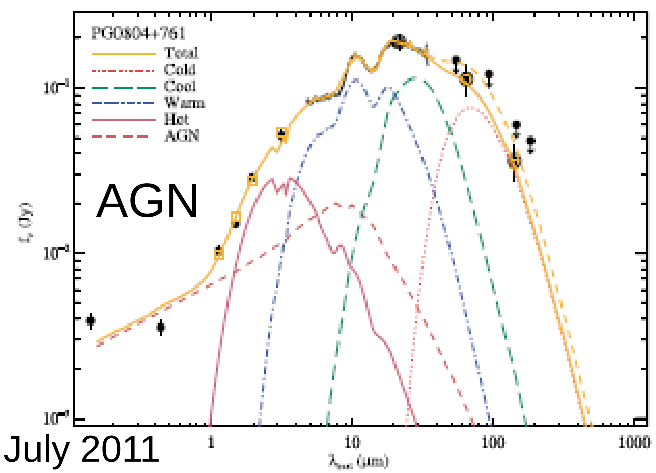

Open circles indicate the position of the MIPS 24 m point to which the IRS spectra are scaled. IRAC and MIPS photometric points are circled.

(Marshall, J.A., et al. 2007, ApJ, 670, 129)

FORCAST

- Two 256x256 arrays:
  - Simultaneous 5-25 & 25-40 micron
- 0.75arcsec/pix
- FOV 3.2 arcmin x 3.2 arcmin
- SWC:
  - 5.4 (0.16)
  - 6.4 (0.14) 6.3 µm PAH feature
  - 6.6 (0.24) 6.6 µm [Ni II] line
  - 7.7 (0.47) 7.7 µm PAH feature
  - 8.6 (0.21) 8.6 µm PAH feature
  - 11.1 (0.95)
  - 11.3 (0.24) 11.3 µm PAH feature
  - 19.7 (5.5)
  - 24.2 (2.9) 24.3 µm [Ne V] line
- LWC:
  - 31.5 (5.7)
  - 33.6 (1.9)
  - 34.8 (3.8) 34.8 µm [Si II] line
  - 37.1 (3.3)

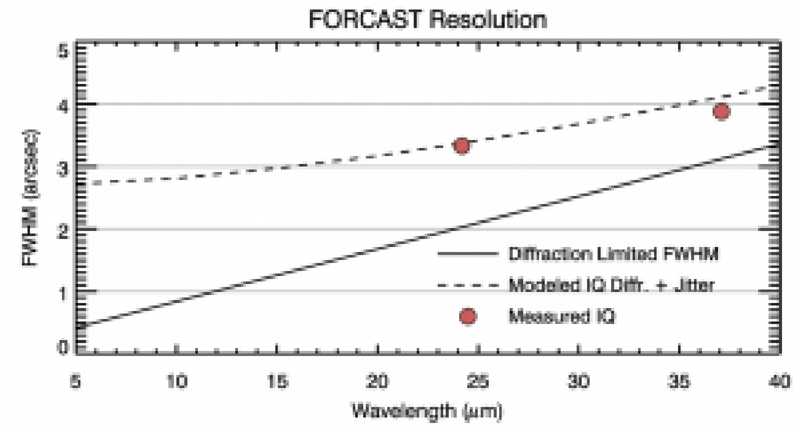

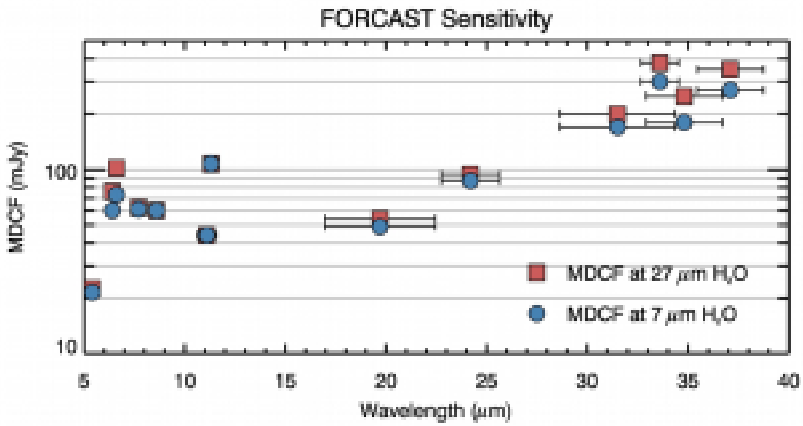

S/N = 4 in 900 sec

Nearby Galaxies: NGC 3227 (I)

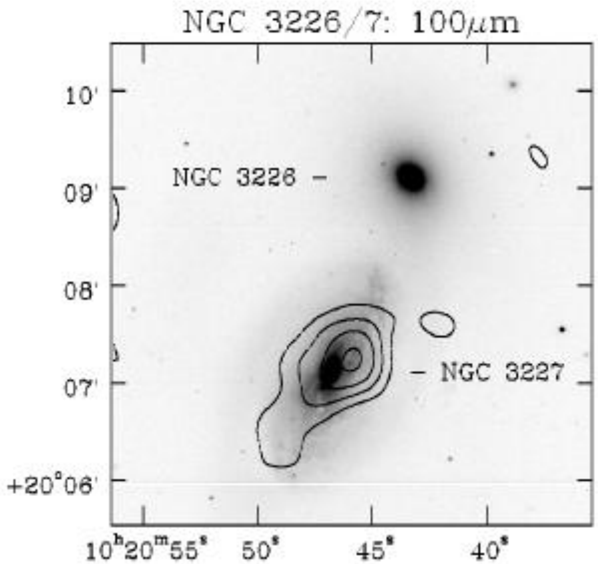

KAO observation

PROPERTIES OF NGC 3227

Property	NGC 3227
Right ascension (J2000)......	$10^h23^m30\overset{s}{.}6$
Declination (J2000)	19°51′53″.99
Classification	SAB(s) pec
Inclination	56°
Position angle	158°
AGN type......................	Seyfert 1.2
Systemic velocity $v_{sys;HI}$	1135 km s^{-1}
Distance	17.3 Mpc
1″ equivalent..................	84 pc

NOTE.—The sky coordinates, the systemic velocity, as well as the Seyfert type were taken from NED (NASA/IPAC Extragalactic Database). The classification is from the RC3 (de Vaucouleurs et al. 1991). Inclination and position angle are taken from Mundell et al. 1995b. For the distance we adopted the value of the LGG 193 group (Garcia 1993) where NGC 3227 is a member.

Schinnerer, Eckart, & Tacconi 2000, ApJ, 533, 826

TABLE 1
GALAXY SAMPLE

GALAXY NGC (1)	GALAXY UGC (2)	SYSTEM TYPE (3)	HUBBLE TYPE (4)	SEPARATION (arcsec) (5)	B_T (mag) (6)	V (km s^{-1}) (7)	ΔV (km s^{-1}) (8)	D (Mpc) (9)	L_B ($10^9 L_\odot$) (10)	L_{IR} ($10^9 L_\odot$) (11)	L_{IR}/L_B (12)
3226/7	5617/20	Pair	E2 + Sb	128	12.3/11.1	1123	177	15	0.6/1.7	3.6	2

Bushouse, Telesco, & Werner 1998, AJ, 115, 938

Nearby Galaxies: NGC 3227 (I)

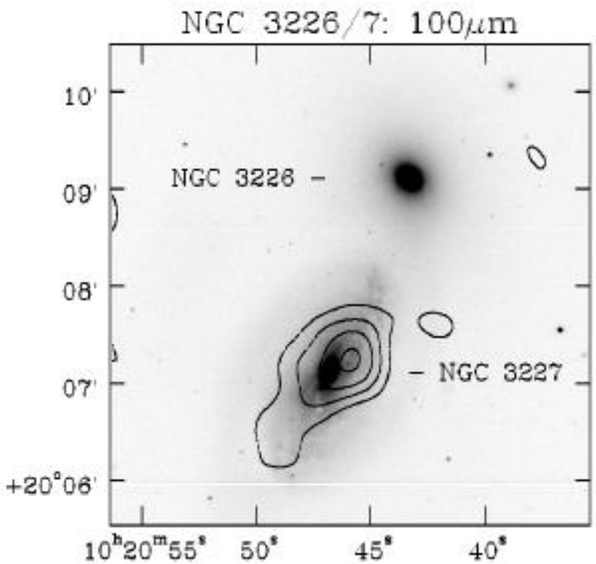

KAO observation

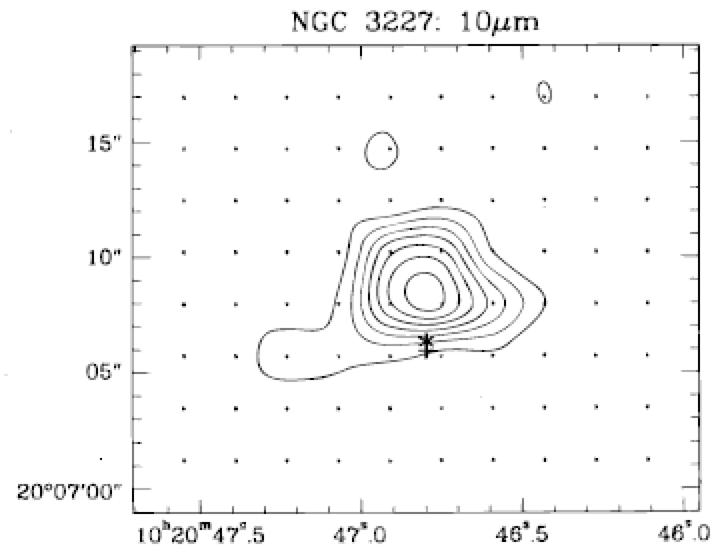

IRTF observation

Bushouse, Telesco, & Werner 1998, AJ, 115, 938

Nearby Galaxies: NGC 3227 (II)

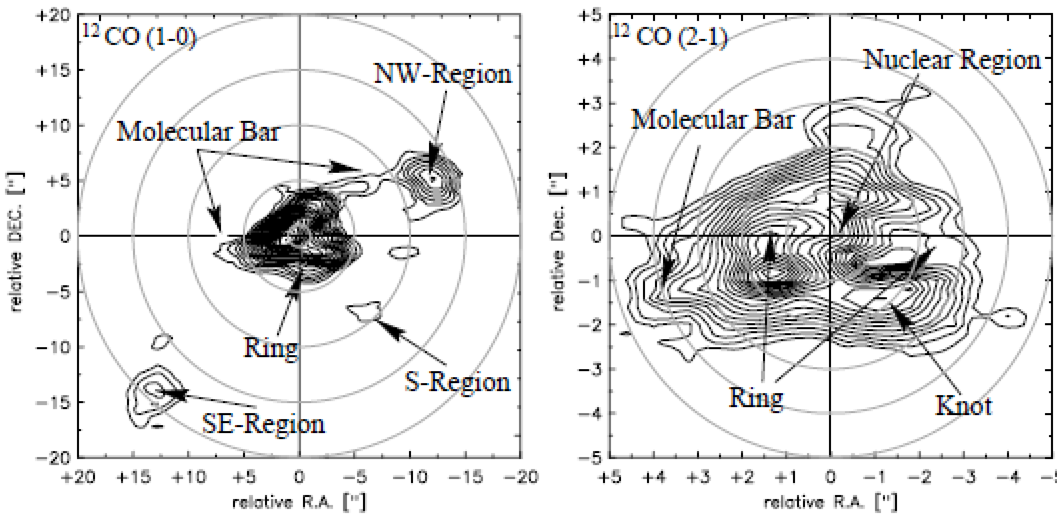

FIG. 2.—Deprojected maps of the PdBI ^{12}CO line emission. The maps are deprojected by correcting for an inclination angle $i = 56°$ and a position angle P.A. $= 158°$. To ease the comparison to the real data, the blue side of the major kinematic axis was aligned to the north. The contours are 5, 10, 15, 20,…, 100% of the peak intensity. The regions discussed in the text are indicated.

Schinnerer, Eckart, & Tacconi 2000, ApJ, 533, 826

Nearby Galaxies: NGC 3227(III)

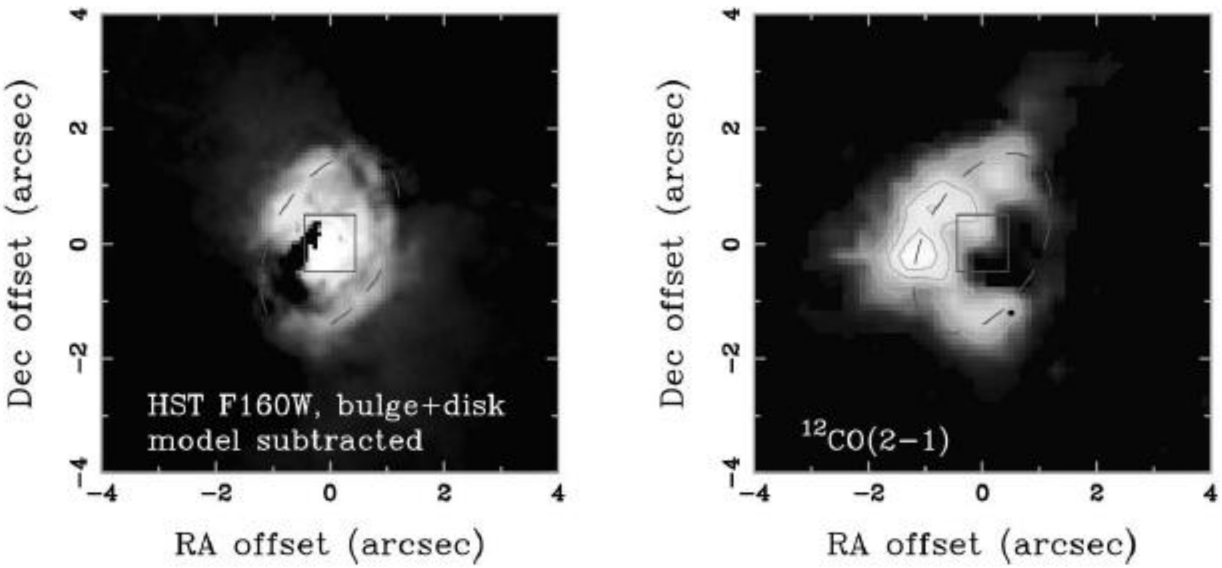

Fig. 2.—Left: HST F160W (square root scaling) image after subtracting the bulge-plus-disk model derived from the 2MASS image and the HST image at r >1.6”. The field of view of SINFONI is shown as a box in the center. The outline of the stellar ring is drawn as a dashed ellipse, with axis ratio 0.6 at a P.A. of -30º. Right: CO(2–1) molecular gas map from Schinnerer et al. (2000), with contours at 40%, 60%, and 80% of the peak. The same box and ellipse as at left are also marked on this image. North is up and east is to the left.

Davies et al. 2006, ApJ, 646, 754

Future SOFIA Observation/Instrumentation

- FORCAST grisms:
  – PAH observation
- FORCAST Fabry-Perot:
  – Mid-IR spectroscopy